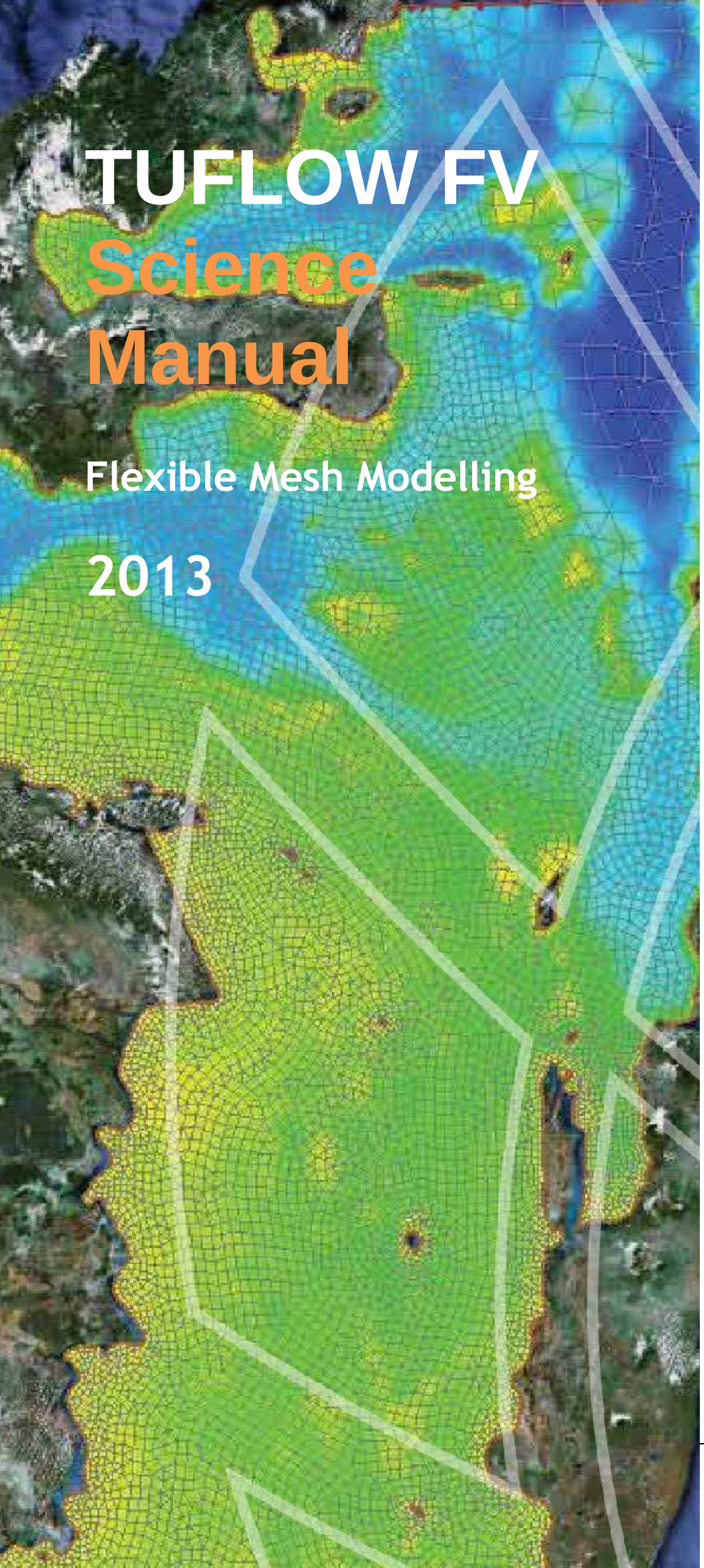

TUFLOW FV
Science Manual

Flexible Mesh Modelling

2013

www.TUFLOW.com
www.TUFLOW.com/forum
wiki.TUFLOW.com
support@tuflow.com

TUFLOW Flood and Tide Simulation Software
BMT WBM

CONTENTS

1 Introduction

TUFLOW FV is a numerical hydrodynamic model for the two-dimensional (2D) and three-dimensional (3D) Non-Linear Shallow Water Equations (NLSWE). The model is suitable for solving a wide range of hydrodynamic systems ranging in scale from the open channels and floodplains, through estuaries to coasts and oceans.

The Finite-Volume (FV) numerical scheme employed by TUFLOW FV is capable of solving the NLSWE on both structured rectilinear grids and unstructured meshes comprised of triangular and quadrilaterial elements. The flexible mesh allows for seamless boundary fitting along complex coastlines or open channels as well as accurately and efficiently representing complex bathymetries with a minimum number of computational elements. The flexible mesh capability is particularly efficient at resolving a range of scales in a single model without requiring multiple domain nesting.

Unstructured mesh geometries can be created using a suitable mesh generation tool. BMT staff generally use the SMS package (http://www.aquaveo.com/sms) for building meshes as well as undertaking a range of model pre-processing and post-processing tasks. Both Cartesian and Spherical mesh geometries can be used as the basis for TUFLOW FV simulations.

Three-dimensional simulations can be performed within TUFLOW FV using either sigma-coordinate or a hybrid z-coordinate vertical mesh. Three-dimensional simulations can optionally use a mode-splitting approach to efficiently solve the external (free-surface) mode in 2D at a timestep constrainted by the surface wave speed while the internal 3D mode is updated less frequently.

Advection-Diffusion (AD) of multiple water-borne constituents can be solved within TUFLOW FV, either coupled with a hydrodynamic simulation, or alternatively in transport mode using a pre-calculated transport file. Simple constituent decay and settling can be accommodated in the AD solutions, or alternatively more complex sediment transport algorithms can be applied through the sediment transport module.

Baroclinic pressure-gradient terms can be optionally activated to allow the hydrodynamic solution to respond to temperature, salinity and sediment induced density gradients. Atmospheric heat exchange can also be calculated given standard meteorological parameter inputs by an integrated module.

TUFLOW FV has a variety of options for simulating horizontal turbulent mixing, including the Smagorinsky scheme. Simple parametric models for vertical mixing are incorporated within TUFLOW FV and for more complicated turbulence model algorithms an interface for linking with various external turbulence models has been implemented.

Both cohesive and non-cohesive sediment transport routines can be accessed through in-built TUFLOW FV modules which handle both bed and suspended load mechanisms. Dynamic morphology updating can be optionally activated.

TUFLOW FV provides a multitude of options for specifying modelboundary conditions, including:

- Various open boundary conditions
- Point source inflows

- Moving point source inflows
- Spatially and temporally varied forcing e.g. windfields, short-wave forcing

2 Non-Linear Shallow Water Equations (NLSWE)

TUFLOW FV solves the the NLSWE, including viscous flux terms and various source terms on a flexible mesh comprised of triangular and quadrilateral elements.

The NLSWE is a system of equations describing the conservation of fluid mass/volume and momentum in an incompressible fluid, under the hydrostatic pressure and Boussinesq assumptions. The standard form of the NLSWE, which relates the time-derivative of the conserved variables to flux-gradient and source terms, is given below.

$$\frac{\partial \boldsymbol{U}}{\partial t} + \nabla \cdot \boldsymbol{F}(\boldsymbol{U}) = \boldsymbol{S}(\boldsymbol{U}) \quad (1)$$

The finite-volume schemes are derived from the conservative integral form of the NLSWE, which are obtained by integrating the standard conservation equation over a control volume, Ω.

$$\int_\Omega \frac{\partial \boldsymbol{U}}{\partial t} d\Omega + \int_\Omega \nabla \cdot \boldsymbol{F}(\boldsymbol{U})\, d\Omega = \int_\Omega \boldsymbol{S}(\boldsymbol{U})\, d\Omega \quad (2)$$

Gauss' theorem is used to convert the flux-gradient volume integral into a boundary-integral:

$$\frac{\partial}{\partial t}\int_\Omega \boldsymbol{U}\, d\Omega + \oint_{\partial\Omega} (\boldsymbol{F} \cdot \boldsymbol{n})\, ds = \int_\Omega \boldsymbol{S}(\boldsymbol{U})\, d\Omega \quad (3)$$

where $\int_\Omega d\Omega$ represent volume integrals and $\oint_{\partial\Omega} ds$ represents a boundary integral and $\boldsymbol{n}$ is the boundary unit-normal vector.

The NLSWE conserved variables are volume (depth),x-momentum and y-momentum:

$$\boldsymbol{U} = \begin{bmatrix} h \\ hu \\ hv \end{bmatrix} \quad (4)$$

where h is depth, u is x-velocity and v is y-velocity.

The x, y and z components of the inviscid flux ($\boldsymbol{F}^I$) and viscous flux ($\boldsymbol{F}^V$) terms in the NLSWE are given below.

$$\boldsymbol{F}_x^I = \begin{bmatrix} hu \\ hu^2 + \frac{1}{2}gh^2 \\ huv \end{bmatrix},\ \boldsymbol{F}_x^V \approx \begin{bmatrix} 0 \\ -hK_v \frac{\partial u}{\partial x} \\ -hK_v \frac{\partial v}{\partial x} \end{bmatrix}$$

$$\boldsymbol{F}_y^I = \begin{bmatrix} hv \\ huv \\ hv^2 + \frac{1}{2}gh^2 \end{bmatrix},\ \boldsymbol{F}_y^V \approx \begin{bmatrix} 0 \\ -hK_v \frac{\partial u}{\partial y} \\ -hK_v \frac{\partial v}{\partial y} \end{bmatrix} \quad (5)$$

$$\boldsymbol{F}_z^I = \begin{bmatrix} hw \\ hwu \\ hwv \end{bmatrix},\ \boldsymbol{F}_z^V \approx \begin{bmatrix} 0 \\ -\nu_t \frac{\partial u}{\partial z} \\ -\nu_t \frac{\partial v}{\partial z} \end{bmatrix}$$

where K_v and υ_t are the horizontal and vertical eddy-viscosity terms.

Some of the various source terms to the NLSWE are provided below:

$$\boldsymbol{S} = \begin{bmatrix} 0 \\ gh\frac{\partial z_b}{\partial x} + fvh - \frac{h}{\rho_0}\frac{\partial p_a}{\partial x} - \frac{hg}{\rho_0}\int_z^\eta \frac{\partial \rho}{\partial x}dz - \frac{1}{\rho_0}\left(\frac{\partial \boldsymbol{s}_{xx}}{\partial x} + \frac{\partial \boldsymbol{s}_{xy}}{\partial y}\right) + \frac{\boldsymbol{\tau}_{sx}}{\rho_0} - \frac{\boldsymbol{\tau}_{bx}}{\rho_0} \\ gh\frac{\partial z_b}{\partial y} - fuh - \frac{h}{\rho_0}\frac{\partial p_a}{\partial y} - \frac{hg}{\rho_0}\int_z^\eta \frac{\partial \rho}{\partial y}dz - \frac{1}{\rho_0}\left(\frac{\partial \boldsymbol{s}_{yx}}{\partial x} + \frac{\partial \boldsymbol{s}_{yy}}{\partial y}\right) + \frac{\boldsymbol{\tau}_{sy}}{\rho_0} - \frac{\boldsymbol{\tau}_{by}}{\rho_0} \end{bmatrix} \quad (6)$$

where,

- $\frac{\partial z_b}{\partial x}, \frac{\partial z_b}{\partial y}$ are the x- and y-components of bed slope;
- f is the coriolis coefficient;
- ρ is the local fluid density, ρ_0 is the reference density and p_a is the mean sea level pressure;
- $\boldsymbol{s}_{ij}$ is the short-wave radiation stress tensor; and
- $\boldsymbol{\tau}_s$ and $\boldsymbol{\tau}_b$ are respectively the surface and bottom shear stress terms (where applicable).

Other source terms not included above include inflow/outflow to/from the water column.

3 Scalar Conservation Equations

Analogous conservation equations are solved for the transport of scalar constituents in the water column.

$$U = [hC] \tag{7}$$

where C is the constituent concentration. The flux components of the scalar conservation equation are:

$$\begin{aligned} F_x^I &= [huC],\ F_x^V \approx \left[-h\left(D_{xx}\frac{\partial C}{\partial x} + D_{xy}\frac{\partial C}{\partial y}\right)\right] \\ F_y^I &= [hvC],\ F_y^V \approx \left[-h\left(D_{yx}\frac{\partial C}{\partial x} + D_{yy}\frac{\partial C}{\partial y}\right)\right] \\ F_z^I &= [hwC],\ F_z^V \approx \left[-h\nu_t'\frac{\partial C}{\partial z}\right] \end{aligned} \tag{8}$$

The source components may include scalar decay and settling:

$$S = [-K_d hC - w_s C] \tag{9}$$

where K_d is a scalar decay-rate coefficient and w_s is a scalar settling velocity.

4 Numerical Scheme

The system of equations described above is solved using a Finite-Volume numerical scheme, as described below. Further details about Finite Volume methods for hyperbolic systems can be found in Leveque (2002).

4.1 Discrete system

The spatial domain is discretised using contiguous, non-overlapping triangular and quadrilateral cells (or elements).

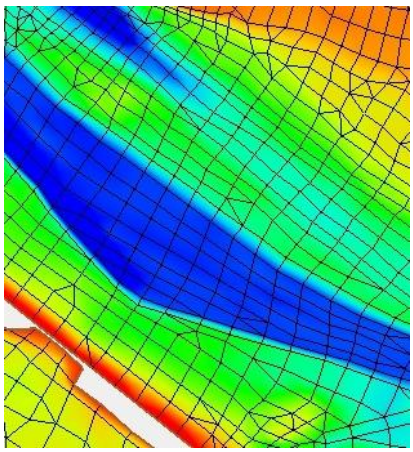

A cell-centred spatial discretisation is adopted for all NLSWE conserved variables. The discrete form of the equations for cell i, with $k = 1, N_k$ cell-faces is:

$$\frac{\partial \boldsymbol{U}_i}{\partial t} = -\frac{1}{A_i}\sum_{k=1}^{Nk}(\boldsymbol{F}_k \cdot \boldsymbol{n}_k)\, L_k + \boldsymbol{S}_i \qquad (10)$$

In this discrete equation $\boldsymbol{U}_i$ represents the volume-average of the conserved variables in cell *i*, A_i is the cross-sectional (plan) area of the cell and $\boldsymbol{S}_i$ is the volume-average source term/s. A first-order midpoint quadrature is used to evaluate the cell boundary flux integral, where $\boldsymbol{n}_k$ is the boundary/face unit normal vector for face *k* and L_k is the corresponding face length. The discrete conserved variable field is assumed to be continuous within a cell but discontinuous at the cell-faces.

The finite-volume form of the conservation equation has delivered an Ordinary Differential Equation (ODE) from the original Partial Differential Equation (PDE) form of the conservation equation (Equation 1). This allows the solution of the conservation system of equations to be separated into a two stage algorithm:

1 the spatial integration of the discrete flux and source components (RHS of Equation 10)

2 the time integration of the discrete system of system of conservation equations

4.2 Spatial Order

The first-order form of the finite volume schemes assumes a piecewise constant $\boldsymbol{U}_i$ within each model cell (Leveque, 2002). Finite-volume schemes with higher-order spatial accuracy can be derived by re-constructing a piecewise continuous $\boldsymbol{U}_i(x, y, z)$ within each model cell. For instance, a second-order

spatial scheme can be derived by re-construction of a piecewise linear $\boldsymbol{U}_i(x, y, z)$, while a third-order spatial scheme would require re-construction of a piecewise parabolic $\boldsymbol{U}_i(x, y, z)$. It should be noted that the discrete $\boldsymbol{U}_i$ remains discontinuous at cell-faces even for schemes higher than first-order (Hubbard, 1999).

The higher spatial orders can significantly reduce numerical diffusion where the physical system being solved includes large spatial gradients relative to the discrete mesh size. Numerical diffusion can also be reduced through selection of a finer mesh resolution, however the higher spatial order schemes will generally achieve this outcome with less increase in computational overhead.

In general, the solution will only benefit from higher spatial order when the spatial gradients become sufficiently large relative to the mesh size. This can only be determined by testing for improvements in the higher-order solution relative to the first-order solution. If the first-order and high-order solutions are more or less identical for the particular model purpose, then it is generally appropriate to adopt the first-order accuracy. However, if the solutions are significantly different this suggests that first-order numerical diffusion is substantial relative to the physical fluxes that are being resolved in the model. In this case the higher-order solution is probably of a higher quality, though care must be exercised with the higher order solutions to ensure that spurious "overshoots" at the cell faces are avoided by the reconstruction procedure.

The Total Variation Diminishing (TVD) property (and hence stability) of the higher-order scheme solution is achieved using a choice of gradient limiter schemes. A variety of gradient limiters are available in TUFLOW FV and are listed in Table 1 in order from least to most "compressive". The most "compressive" schemes will maximise the resolution of sharp gradients but may do so at the expense of additional computational overhead. The most compressive gradient limiter schemes also increase the risk of generating spurious "overshoots" within the solution.

Within TUFLOW FV horizontal and vertical reconstructions are performed separately. A first-order horizontal reconstruction can be combined with a second-order vertical reconstruction, and vice-versa.

Table 1 Overview of gradient limiter schemes applied in TUFLOW FV

	Horizontal gradient limiter scheme	Vertical gradient limiter scheme
Least Compressive		MINMOD Fringer et al. (2005)
↓	Limited Central Difference (LCD) Batten et al. (1996)	Maximum Central Fringer et al. (2005)
Most Compressive	Maximum Limited Gradient (MLG) Batten et al. (1996)	Superbee Fringer et al. (2005)

4.3 Mode Splitting

Efficient integration of the NLSWE is achieved through a mode splitting scheme, whereby different components of the governing equations are updated using an appropriate timestep selected by taking into account physical and numerical convergence and stability considerations (e.g. Shchepetkin & McWilliams, 2005).

A reduced set of equations comprising all terms other than the barotropic (or free-surface) pressure-gradients is initially partially solved. As part of this solution, an appropriate "internal mode" timestep is calculated that obeys both:

- Courant-Freidrich-Levy (CFL) constraints imposed by the advective current speeds
- Peclet number (Pe) constraints imposed by the diffusion terms

Prior to updating (or time-integrating) the solution an "external mode" loop is entered, in which a 2D depth-averaged reduction of the 3D NLSWE is solved multiple times, using a timestep that obeys the barotropic Courant-Freidrich-Levy (CFL) constraint imposed by the shallow water wave speed $\bar{u} \pm \sqrt{gh}$ (where $\bar{u}$ is the depth-averaged current speed). The external mode loop is repeated until the cumulative timestep is approximately equal to the internal mode timestep.

The depth-averaged inviscid fluxes from the external mode solution are then used to correct the internal mode inviscid fluxes so that they now represent the total inviscid flux for the 3D solution. The corrected fluxes are used to update the full 3D solution.

A stability constraint imposed by the baroclinic internal wave speed is not explicitly calculated and in some instances may not be automatically met by the mode splitting scheme. This can be addressed by the user reducing the upper-limiting timestep, where oscillations in the pycnocline are seen to be generating numerical instabilities.

Viscous fluxes and both inviscid and viscous scalar transport fluxes are calculated only for the "internal mode" (outer) loop.

Mode splitting can be disabled for 2D simulations and this configuration can be more computationally efficient for fast, shallow flow scenarios where the "internal mode" and "external mode" timesteps are similarly restrictive.

Currently, 3D simulations are only supported with mode splitting enabled.

4.4 Flux Terms

A key step in the Finite-Volume numerical scheme is the calculation of numerical fluxes across cell boundaries:

- invsicid fluxes ($\boldsymbol{F}_x^I, \boldsymbol{F}_y^I, \boldsymbol{F}_z^I$) represent the directly resolved flux of mass and momentum between adjacent cells
- viscous fluxes ($\boldsymbol{F}_x^V, \boldsymbol{F}_y^V, \boldsymbol{F}_z^V$) represent the "mixing" of mass and momentum that is not directly resolved as advection within the numerical model

4.4.1 Viscous Fluxes

Viscous flux terms are calculated using the traditional gradient-diffusion model with a variety of options available for the calculation of eddy-viscosity and scalar diffusivity.

4.4.1.1 Horizontal viscous fluxes

The horizontal viscous fluxes $(\boldsymbol{F}_x^V, \boldsymbol{F}_y^V)$ are calculated according to Equations 5 and 8. The horizontal eddy-viscosity can be specified directly or can be calculated from the Smagorinsky formulation below.

$$K_v = {c_s}^2 {l_s}^2 \sqrt{\left(\frac{\partial u}{\partial x}\right)^2 + \left(\frac{\partial v}{\partial y}\right)^2 + \frac{1}{2}\left(\frac{\partial u}{\partial y} + \frac{\partial v}{\partial x}\right)^2} \quad (11)$$

where c_s is the Smagorinsky coefficient and l_s is the Smagorinsky lengthscale which is related to the local mesh size.

The horizontal scalar-diffusivity tensor can also be specified directly (as an isotropic constant value) or can be calculated from a Smagorinsky formulation (Eq. 11) or from the "Elder" formulation below (Falconer et al., 2005). The Elder model calculates a non-isotropic diffusivity tensor that accounts for velocity dispersion processes not resolved in 2D depth-averaged models.

$$\begin{aligned} \mathbf{D}_{xx} &= (D_l u^2 + D_t v^2)\mathrm{h}/u_* \\ \mathbf{D}_{yy} &= (D_l v^2 + D_t u^2)h/u_* \\ \mathbf{D}_{xy} &= \mathbf{D}_{yx} = (D_l - D_t)uvh/u_* \end{aligned} \quad (12)$$

and D_l, D_t are the Elder coefficients in the directions lateral to the local current and transverse to the local currents respectively and $u_* \left(= \sqrt{|\boldsymbol{\tau}_b|/\rho}\right)$ is the friction velocity. The observed range of values for D_l, D_t derived from measurements are discussed in Fisher et al., 1979.

In 3D model simulations the Smagorinsky formulation is generally more applicable.

4.4.1.2 Vertical viscous fluxes

The vertical viscous fluxes $\boldsymbol{F}_z^V$ are calculated according to Equations 5 and 8. An unconditionally stable semi-implicit scheme is adopted in the discretisation of $\boldsymbol{F}_z^V$ in order to avoid these terms imposing restrictions on the model timestep.

The vertical eddy viscosity, ν_t, can be directly specified or may be calculated from the simple parametric model formulation including Munk & Anderson (1948) stability function:

$$\nu_{t0} = \kappa u_* z \left(c_1 - c_2 \frac{z}{h}\right) \quad (13)$$

$$\nu_t = \sqrt{1 + 10.Ri}\, \nu_{t0} \quad (14)$$

where Ri is the gradient Richardson number defined as,

$$Ri = \frac{N^2}{(\partial u/\partial z)^2} \quad (15)$$

And N is the Brunt-Vaisala frequency (or buoyancy frequency)

$$N = \sqrt{-\frac{g}{\rho}\frac{\partial \rho}{\partial z}} \quad (16)$$

The scalar diffusivities, ν_t', may also be directly specified or it may be calculated using the parametric model formulations below, which vary depending on scalar type:

Passive tracers: $$\nu_t' = \nu_t$$

Temperature and salinity $$\nu_t' = \begin{cases} \frac{1}{\sigma}\nu_t \, (1. + 3.33Ri)^{-1.5} & Ri > 0. \\ \frac{1}{\sigma}\nu_t & Ri \leq 0 \end{cases} \quad (17)$$

Sediment fractions $$\nu_t' = \beta \, \nu_t$$

Where σ is the neutral turbulent Prandtl number and β is the sediment mixing coefficient.

4.4.2 Inviscid Fluxes

Invsicid fluxes ($\boldsymbol{F}_x^I, \boldsymbol{F}_y^I, \boldsymbol{F}_z^I$) represent the directly resolved flux of mass and momentum between adjacent cells.

Inviscid fluxes are calculated for each cell-face based upon the conserved variable state immediately on either side of the cell-face.

For the first-order spatial scheme these values are equivalent to the adjacent-cell-averages, whereas the higher-order schemes will have reconstructed the conserved variable state at the cell-faces from the cell-averages.

4.4.2.1 Internal Mode

The "internal mode" inviscid flux calculations solve the full 3D NLSWE, excluding the terms related to the free-surface pressure gradient. A centred scheme is used to evaluate the internal mode mass flux while an upwind scheme is used for the momentum flux terms. "Flux-like" source terms originating due to bed slope and from the baroclinic pressure gradients are included in the cell-face flux calculation rather than included in the volume-integrated source term in Equation 10 .

The stable internal mode timestep is dictated by internal advection CFL constraints in combination with viscous flux Peclet constraints. A stable internal mode timestep is selected prior to entering the external mode.

4.4.2.2 External Mode

The "external mode" inviscid flux calculations solve the 2D depth-averaged NLSWE. For 3D simulations, the external mode is initiated by calculating depth-averages of the 3D conserved variable fields. Viscous fluxes and baroclinic pressure gradients are also depth-integrated at the start of the external mode loop.

The 2D depth-averaged NLSWE are solved using Roe's approximate Riemann solver (Roe, 1981). "Flux-like" source terms originating due to bed slope and from the depth-averaged baroclinic pressure gradients are included in the cell-face flux calculation rather than included in the volume-integrated source term in Equation 10 (refer Section 4.7).

The stable external mode timestep is dictated by the surface gravity wave CFL constraint in combination with the depth-averaged viscous flux Peclet constraints (Murillo et al., 2005). A stable external mode timestep is selected at each external mode sub-timestep. Within the external mode loop, multiple sub-timesteps are executed prior to returning to the outer "internal mode" loop.

4.4.2.3 Flux Correction

The "internal mode" inviscid fluxes are corrected using the depth-averaged "external mode" fluxes that have been integrated in time through the external mode loop.

When mode splitting is optionally disabled, the complete NLSWE (including free-surface pressure gradients) are solved directly using the same NLSWE flux scheme described for the External Mode calculation. This option is currently only available for 2D model simulations, and can be more computationally efficient than the mode split scheme for pure hydrodynamic simulations of relatively fast shallow flows.

4.4.2.4 Scalar Inviscid Fluxes

Scalar inviscid fluxes are calculated from the product of the "corrected" mass flux and the upwind cell-face concentration. Knowing the "corrected" horizontal inviscid fluxes the vertical inviscid fluxes are simply calculated from the continuity equation.

4.4.3 Total Flux

The total flux vector is simply the sum of the corrected inviscid and viscous flux components.

4.4.4 Flux Spatial Integration

The first term on the RHS of Equation 10 requires calculating the boundary-integral of the total flux vector normal component and is approximated using a simple midpoint quadrature rule.

The momentum flux terms are first converted to a momentum flux difference prior to the integration step. In the case of spherical coordinates the momentum and flux vectors are shifted from a face-centred to cell-centred basis by applying a "parallel transport" transformation. This accounts for rotation of the spherical coordinates vector basis during translation on the sphere (Rossmanith, 2004).

4.5 Time integration

Both internal mode and external mode temporal integration is performed with an explicit Euler scheme. Accordingly a stable time step must be bounded by the Courant-Friedrich-Levy (CFL) criterion for the wave propagation and advective terms and by the Peclet criterion for the diffusive terms (Murillo et al., 2005).

The external mode CFL criterion is given by:

$$\frac{|\mathbf{u}\cdot\mathbf{n}\pm\sqrt{gh}|\Delta t}{L^*} \leq 1 \quad (18)$$

where Δt is the integration timestep and L^* is a cell-size dependent length scale.

The internal mode CFL criterion is given by:

$$\frac{\max(|\mathbf{u}\cdot\mathbf{n}|,c_{baro})\Delta t}{L^*} \leq 1 \quad (19)$$

where c_{baro} is the baroclinic (internal) wave speed.

The Peclet criterion is given by:

$$\frac{|\mathbf{D}\cdot\mathbf{n}|\Delta t}{L^{*2}} \leq 1 \quad (20)$$

In the above stability criterion relationships the cell-size dependent length-scale L^* is calculated for each cell-face as:

$$L^* = \frac{\min(A_i,A_j)}{L_k} \quad (21)$$

where A_i, A_j are the adjacent cell-areas and L_k is the face length.

A variable time step scheme is implemented to ensure that the CFL and Peclet criterion are satisfied at all points in the model with the largest possible time step. Outputs providing information relating to performance of the model with respect to the CFL criterion are provided to enable informed refinement of the model mesh in accordance with the constraints of computational time (refer TUFLOW FV user manual for details).

In stratified flows the baroclinic wave speed may impose a constraint on the stable internal mode timestep as shown in Eq. 19. However, the FV internal mode timestep is not automatically adjusted to satisfy the baroclinic wave speed limit. Additionally the mode splitting scheme stability may benefit from limiting the ratio between the internal and external mode timstep to around 10 or less.

Maximum and minimum timestep limits are specified by the user. The maximum limit should be used to limit the upper internal mode timestep. The minimum limit should be used to restrict the external mode timestep in the event of a model instability, as it is preferable to have the model violate the prescribed stability bounds than have the timestep decrease towards zero.

4.6 Wetting/Drying

In very shallow regions (~<0.05m depth), the momentum terms are dropped, in order to maintain stability as the NLSWE approach the zero-depth singularity. Mass conservation is maintained both locally and globally to the limit of numerical precision across the entire numerical domain, including wetting and drying fronts. A conservative mass re-distribution scheme is used to ensure that negative depths are avoided at numerically challenging wetting and drying fronts without recourse to adjusting the time step (Brufau et al., 2004; Murillo, 2006). Regions of the model domain that are effectively dry are readily dropped from the computations.

4.7 Source terms

4.7.1 Bed slope

Bed slope integral source terms are calculated using a face-centred "upwind flux correction" within the internal and external mode numerical flux solvers.

$$\int_{\Omega} -gh\nabla \mathbf{z_b} \partial\Omega \cong \sum_{k=1}^{N_k} \beta^*(\Delta z_b)_k \, L_k \qquad (22)$$

That is the cell-face bed elevation jump (Δz_b) becomes a correction term $\beta^*(\Delta z_b)$ to the cell-face numerical flux terms. This numerical approach provides consistent upwinding between flux and bed-slope source terms. This is essential to obtaining the required numerical balance between these terms, at for instance the quiescent state equilibrium.

Further details are provided in the following references; Hubbard & Garcia-Navarro, 2000; Murillo, 2006.

4.7.2 Coriolis

Coriolis forces due to the earth's rotation are calculated as cell-averaged source terms in the momentum equation. The coriolis coefficient f_c is calculated from:

$$f_c = 2\Omega_r \phi \qquad (23)$$

where Ω_r is the angular frequency of the earth's rotation (rad/s)and ϕ is the geographic latitude (radians).

For Cartesian coordinate system models the latitude is specified as a domain constant value. In spherical coordinate models the latitude is obtained locally from the y-coordinate value.

4.7.3 Wind Stress

The cell-averaged surface stress vector due to wind is calculated from

$$\boldsymbol{\tau}_{sw} = \rho_a c_{dw} \mathbf{u}_w |\mathbf{u}_w| \qquad (24)$$

where the wind drag coefficient is calculated using the empiral formula of Wu (1980; 1982)

$$c_{dw} = \begin{cases} c_a & w_{10} < w_a \\ c_a + \frac{c_b - c_a}{w_b - w_a}(w_{10} - w_a) & w_a \le w_{10} < w_b \\ c_b & w_{10} \ge w_b \end{cases} \qquad (25)$$

With default parameters (wa; ca; wb; cb) = (0.0; 0.8e-3; 50.0; 4.05e-03).

4.7.4 Bed Friction

Bed friction momentum sink terms are calculated using a quadratic drag law.

$$\boldsymbol{\tau}_{bf} = \rho c_{db} \mathbf{u} |\mathbf{u}| \qquad (26)$$

where the bottom drag coefficient can be calculated using a roughness-length relationship:

$$c_{db} = \left(\frac{\kappa}{\ln(30.z\prime/k_s)}\right)^2 \quad (27)$$

The above relationship is based on the assumption of a rough-turbulent logarithmic velocity profile in the lowest model layer, where κ is von Karman's constant, k_s is the effective bed roughness length (equivalent Nikuradse roughness) and z' is the height of the bottom cell-centroid above the seabed.

Instead of specifying k_s a Manning's *n* roughness can be specified and is internally converted into an equivalent roughness length:

$$k_s = 15.h \exp\left(-\frac{\kappa h^{1/6}}{\sqrt{g}n}\right) \quad (28)$$

Bed roughness values (k_s: or Manning's *n*) may be specified globally or for "material" types as defined in the mesh geometry file.

The above bed friction formulations are generally applicable in both 2D (depth-averaged) and 3D configurations. In 2D situations the Manning's *n* formulation (Eqs. 27and 28) is equivalent to the following equation for the friction slope (Chow, 1959).

$$\mathbf{S}_f = \frac{\boldsymbol{\tau}_{bf}}{\rho g h} = \frac{n^2 \bar{\mathbf{u}}|\bar{\mathbf{u}}|}{h^{4/3}} \quad (29)$$

It should be noted that given the same bed-roughness parameters calculated bed friction energy losses are typically not exactly equivalent for 2D and 3D simulations except in the simplest fully-developed, uniform flow scenarios. This is because the 2D models "assume" a logarithmic velocity profile extending over full-depth, whereas 3D simulations resolve the vertical velocity profile,which may be non-logarithmic in complex flow situations.

Integrated bed friction source terms are calculated using a semi-implicit discretisation in order to maintain unconditional numerical stability of these terms in high-velocity or shallow flows (Brufau et al, 2004). Coupling of the internal/external modes is achieved by applying the internal mode (3D) bed friction as an explicit momentum sink/source term during external mode (2D) loop calculations.

4.7.5 Surface Friction

Surface friction (e.g. from ice or pontoon structures) can be applied using a quadratic drag law analogous to Equation 26.

Only a roughness length input (k_s) is supported for surface friction specification. It should be noted that the surface friction terms are calculated explicitly and therefore do not exhibit the same unconditional stability property as the bed friction terms. In some circumstances these terms may generate numerical instabilities in high-velocity or shallow flows, which can be treated with a timestep reduction.

Surface roughness values may be specified globally or for "material" types as defined in the mesh geometry file.

4.7.6 Mean Sea Level and Baroclinic Pressure Gradients

Mean Sea Level Pressure and Baroclinic pressure gradient source terms are calculated as a face-centred flux correction terms within the internal and external mode numerical flux solvers. That is the pressure gradient terms are treated in a similar manner to the bed slope source terms as described in Section 4.7.1, i.e.

$$\int_{\Omega} -(\nabla P)\partial\Omega \cong \sum_{k=1}^{N_k} \eta^*(\Delta P)_k \, L_k \qquad (30)$$

where ∇P is the gradient of the combined atmospheric and baroclinic pressure fields and η^* is a face-centred flux correction due to the cell-face pressure jump ΔP. This is analogous to converting the cell-volume source term integral into a cell-boundary source term integral using Gauss' theorem.

4.7.7 Wave radiation stress

Wave fields are applied as spatially and temporally varying datasets on a 2D rectilinear/curvilinear grid. The wave field boundary condition data is specified in a netcdf file and applied to the TUFLOW FV model as described in the user manual.

Wave radiation stress gradients are calculated as cell-centred source terms:

$$\int_{\Omega} \left(\frac{\partial \boldsymbol{s}_{xx}}{\partial x} + \frac{\partial \boldsymbol{s}_{xy}}{\partial y}\right) \partial\Omega \qquad (31)$$

or as face-centred momentum flux source terms.

The wave radiation stress gradients are currently distributed uniformly throughout the water column. More advanced options will be implemented in future release/s of the software.

4.7.8 Scalar Decay

Tracer constituents can be specified with a linear scalar decay property (Equation 9), where K_d is the constant linear decay coefficient. Scalar decay is discretised explicitly as a cell-centred integral source term.

Numerical stability of this term is not guaranteed for large K_d or for large model timesteps.

4.7.9 Scalar (Sediment) Settling

Tracer and sediment constituents can be specified with a settling velocity w_s (Equation 9).

Within the water column, the settling velocity contributes an additional (vertically downward) inviscid flux component. At the seabed the settling velocity contributes a sink from the water column and source into the bed. In the case of sediment fractions the mass transferred to the bed is subsequently tracked within the TUFLOW FV sediment module. The passive tracer constituent mass exiting the water column is no longer tracked.

4.7.10 Other Sources/Sinks

Inflows/outflows into/from model domain can be specified as boundary conditions to the model. These boundaries typically require specification of the volumetric flow rate (inflow = +ve, outflow = -ve) and associated scalar concentrations.

In the case of an outflow specification, either the internal domain concentration (at the extraction location) can be applied (this is the default) or alternatively the outflow concentration can be directly specified. The latter approach might be used to simulate evaporation from the water column, where there is no scalar mass loss corresponding to the volumetric loss, i.e. the outflow concentration for the scalar constituents is zero. Another option, where there is no volumetric source, is to directly specify the scalar mass fluxes.

The spatial definition of source/sink boundary conditions, includes the following options as described in the user manual:

- Global (spatially constant and variable) source/sinks
- Point source/sinks
- Moving point source/sinks

The vertical distribution of the source/sink terms can be specified as part of the boundary condition definition. A detailed description of the available source/sink boundary condition options is provided in the TUFLOW FV user manual.

The TUFLOW FV sediment module calculates the sediment settling/mixing parameters and bed-pickup sink/source terms required as inputs and boundary conditions to the suspended sediment advection/dispersion calculations. Additionally this module can calculate bed load transport and bed-elevation update in response to sediment transport gradients.

The TUFLOW FV atmospheric module calculates the transfer of mass/heat/momentum between the water column and the atmosphere.

4.8 Timestep Algorithm

The timestep algorithm within TUFLOW FV is summarised in the following flowchart.

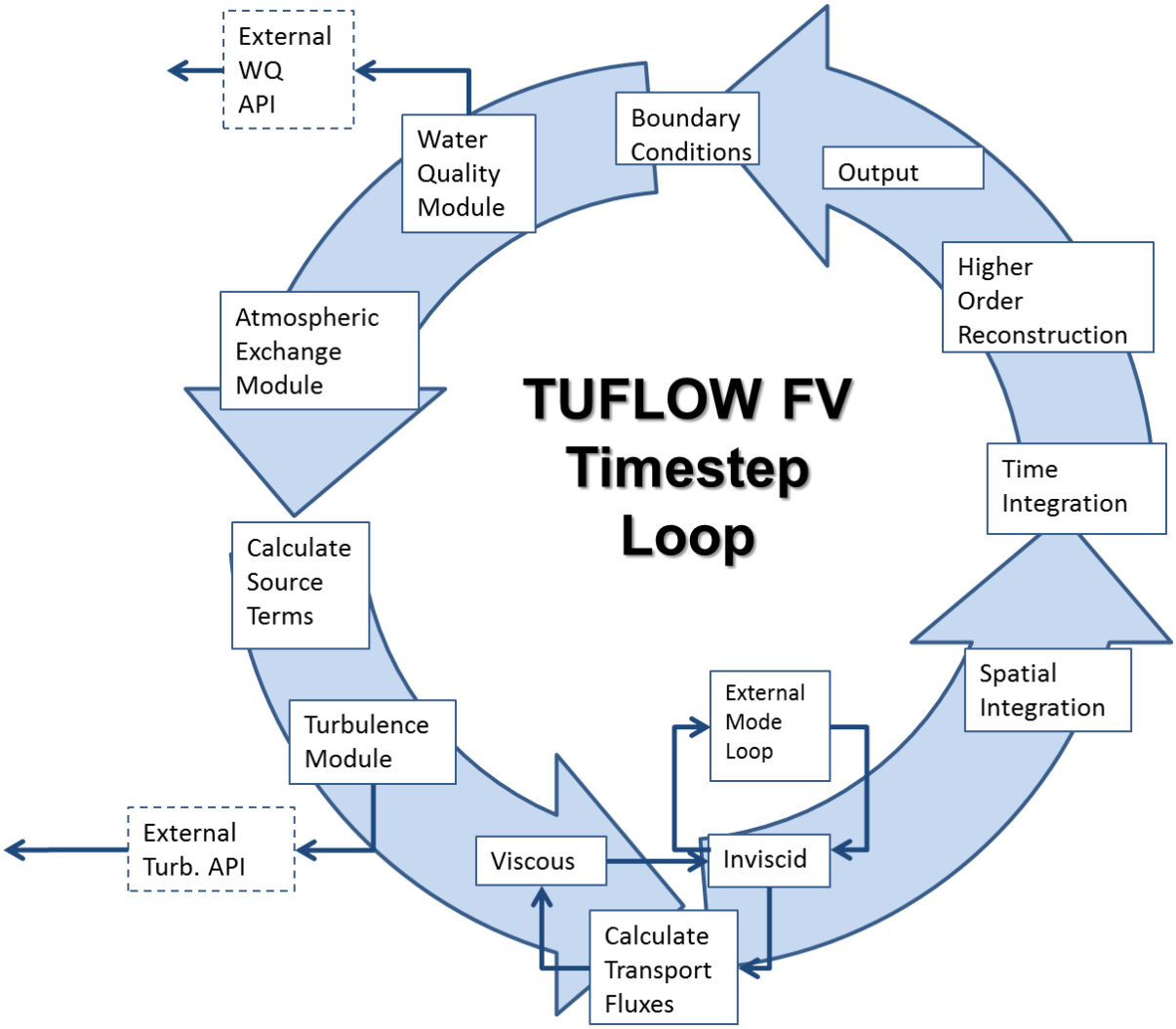

Figure 1 TUFLOW FV timestep loop illustration (further details outlined in Table 2)

Table 2 TUFLOW FV timestep algorithm

• Write output • Update Boundary Condition data • Do Water Quality calculations • Do Sediment Transport calculations • Do atmospheric exchange calculations • Reset source terms • Update cell-centred boundary conditions • Update structure flows • Calculate horizontal and vertical turbulent viscosities & diffusivities • Calculate density • Calculate cell-face pressure differences (due to MSLP and baroclinic gradients) • Calculate internal mode inviscid fluxes • Calculate viscous fluxes • Calculate cell-centred source terms • Determine internal mode timestep	
• Enter external mode loop, initialising external mode variables	
	• Calculate external inviscid flux • Determine external mode timestep • Integrate the external inviscid flux wrt time • Calculate total external mode • Spatially integrate external mode fluxes • Perform conservative mass redistribution • Perform time integration • Update external mode sub-timestep • Apply ghost-cell boundary conditions • Calculate primitive variables • Update nodal values • Calculate face-centred gradients • Higher order scheme reconstruction (if required) • Update cell-face values • Update wet/dry flags
• Exit external mode loop and perform internal mode flux corrections	
• Calculate horizontal scalar inviscid fluxes • Calculate total horizontal fluxes • Spatially integrate horizontal fluxes • Calculate depth change (time integrate depth-averaged continuity equation) • Calculate vertical fluxes (inviscid and viscous) • Perform time integration • Update timestep • Apply ghost-cell boundary conditions • Calculate primitive variables • Update nodal values • Calculate face-centred gradients • Higher order scheme reconstruction (if required) • Update cell-face values • Update wet/dry flags • Check model bounds	

5 Benchmarking

A range of benchmark tests have been conducted to prove TUFLOW FV performance, including 2D and 3D tests. The following contains a selection of these tests; documentation of further tests can be provided upon request. Please contact support@tuflow.com for more information.

5.1 2D benchmarks

5.1.1 Carrier et al 2003 Initial Value Problem

In this problem an initial offshore water surface profile is specified (Figure 1) on an uniform 1:10 slope. The initial water velocity throughout the problem domain is zero. The initial-value-problem (IVP) technique introduced by Carrier, Wu and Yeh (2003) is used to produce the benchmark data. The benchmark task is to produce snapshots of the free surface and velocity profiles at t = 160s, 175s, and 220s. These comparisons are shown in Figures 2 and 3. In addition, the trajectory of the shoreline is plotted in Figure 4. It is noted that the results from the TUFLOW FV model are in close agreement with the benchmark solution in all cases.

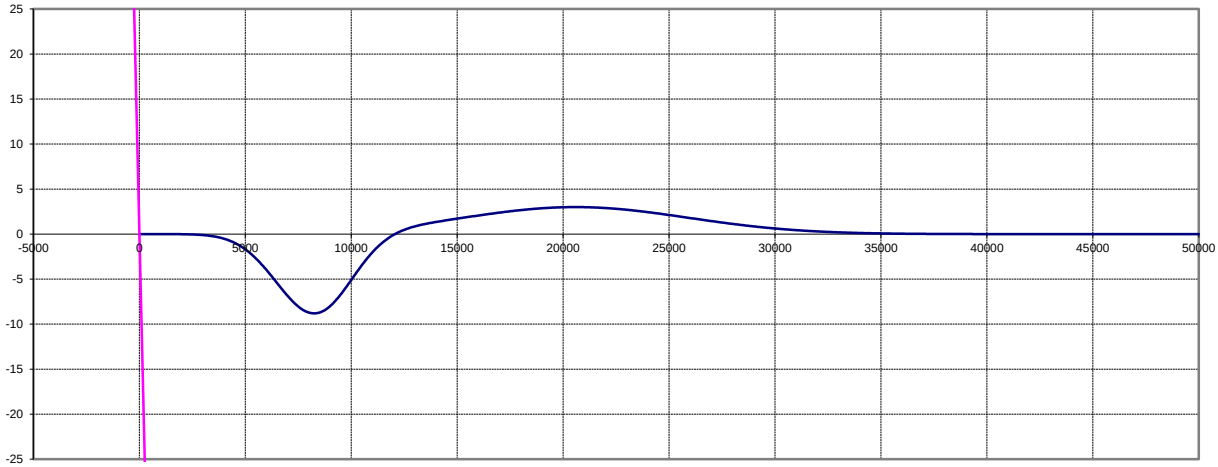

Figure 1 Initial water surface elevation plot at t = 0s

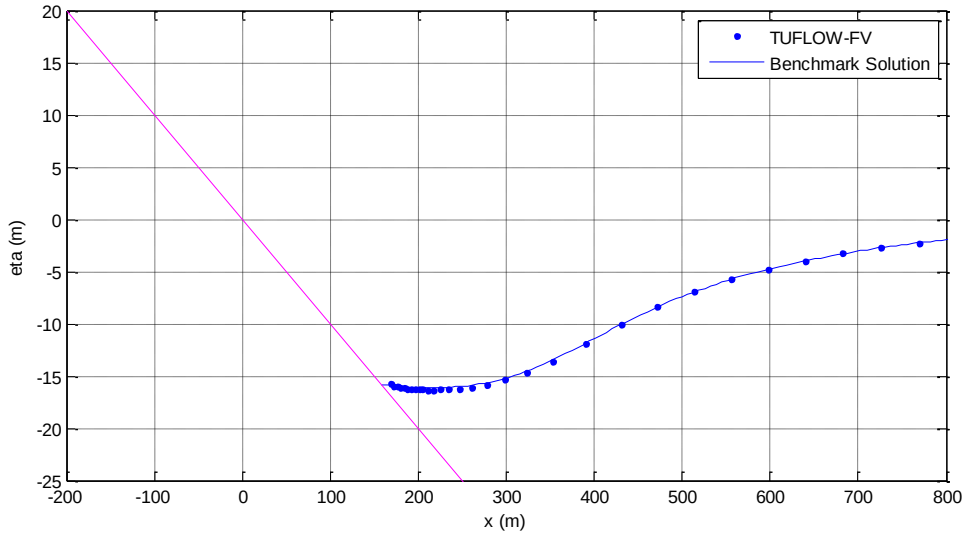

(a) t = 160s

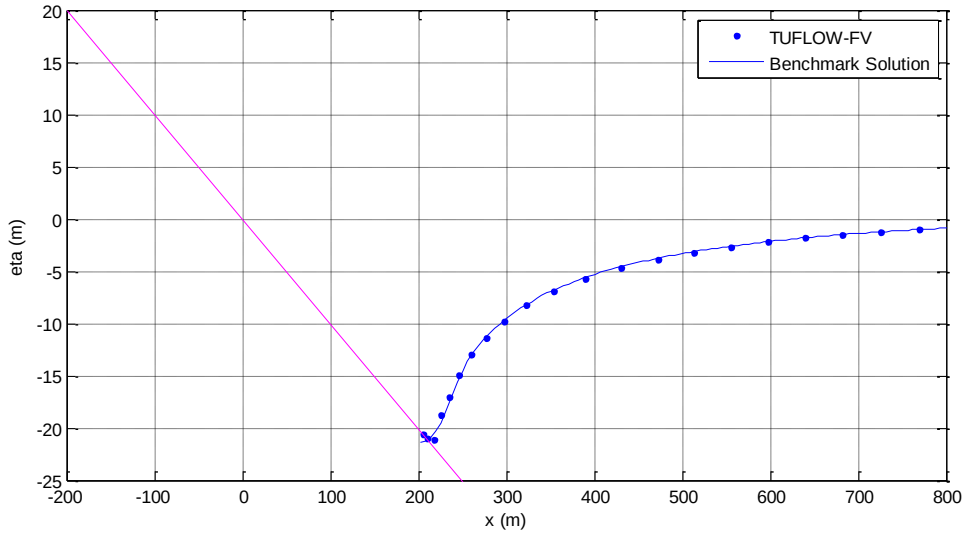

(b) t = 175s

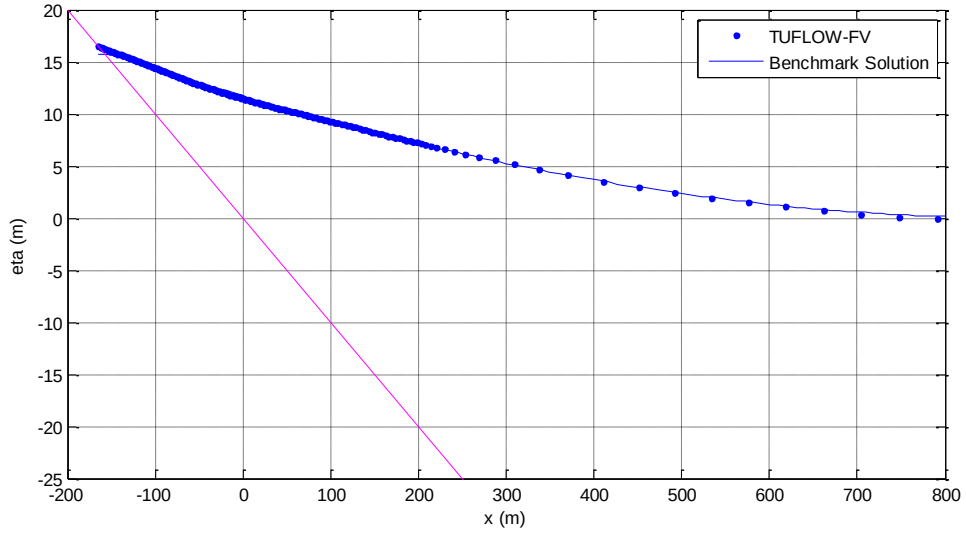

(c) t = 220s

Figure 2 Snapshots of water surface elevation at (a) 160s, (b) 175s and (c) 220s

5.1.2 Monai Valley, Okushiri Island

The 1993 Okushiri tsunami caused a runup of 32 m near the village of Monai in Okushiri Island. This tsunami runup mark was discovered at the tip of a very narrow gulley within a small cove. This benchmark problem is a 1/400 scale laboratory experiment of the Monai runup, using a large-scale tank (205 m long, 6 m deep, 3.4 m wide) at Central Research Institute for Electric Power Industry (CRIEPI) in Abiko, Japan. The benchmark task is to reproduce the results of the laboratory experiment. Figure 5 shows the bathymetry and coastal topography used in the laboratory experiment, as well as the timeseries of water level prescribed at the offshore boundary. The other three boundaries are reflective sidewalls. The numerical model is required to reproduce the temporal and spatial variations of the shoreline location, as well as the temporal variations of the water-surface variations at three specified nearshore locations (marked ch5, ch7 and ch9 in Figure 5). Figures 6 and 7 illustrate the good performance of the model compared to the laboratory experimental results.

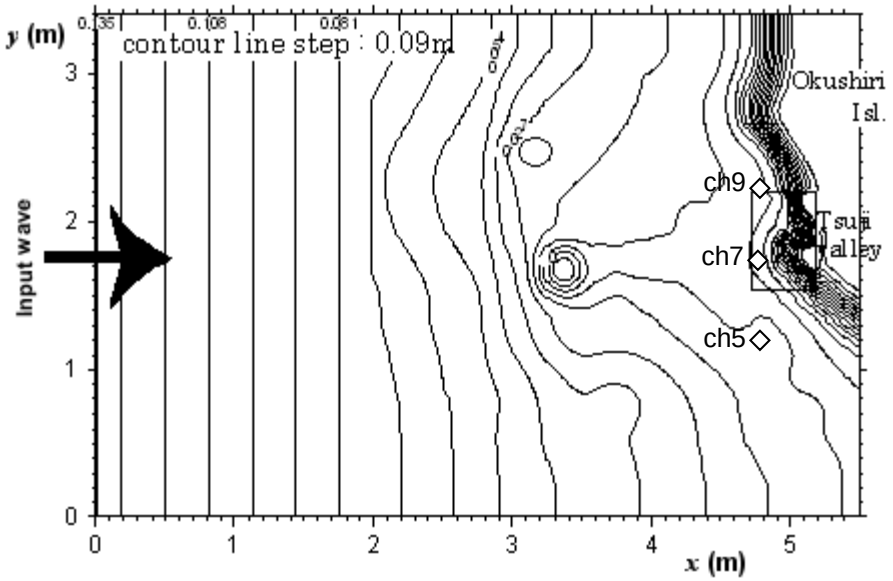

Input wave timeseries:

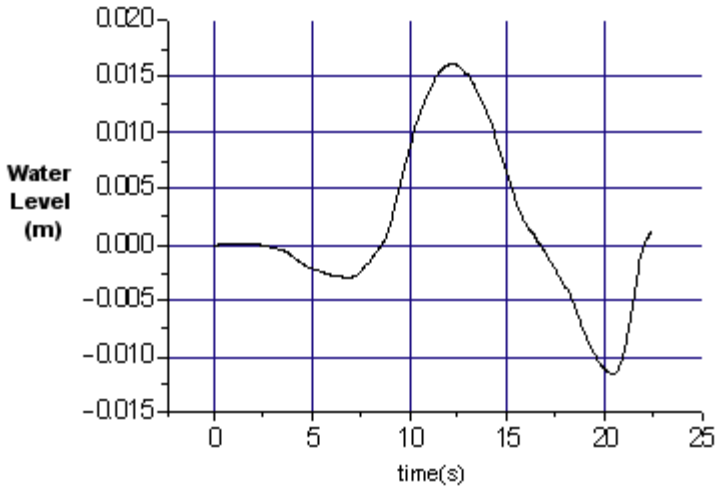

Figure 5 The laboratory experiment bathymetry and the water surface timeseries boundary condition

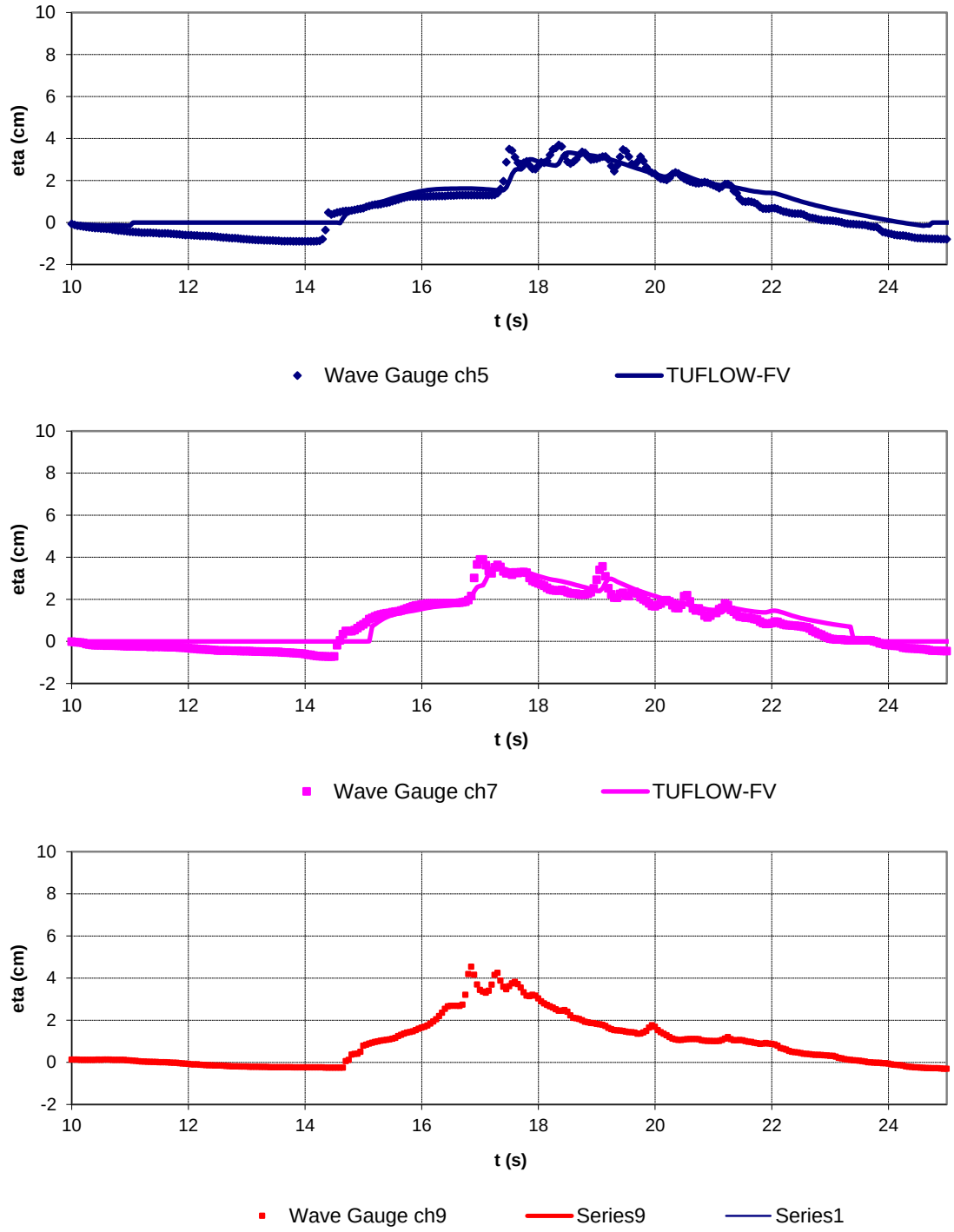

Figure 6 Timeseries of water surface elevation at wave gauges ch5, ch7 and ch9

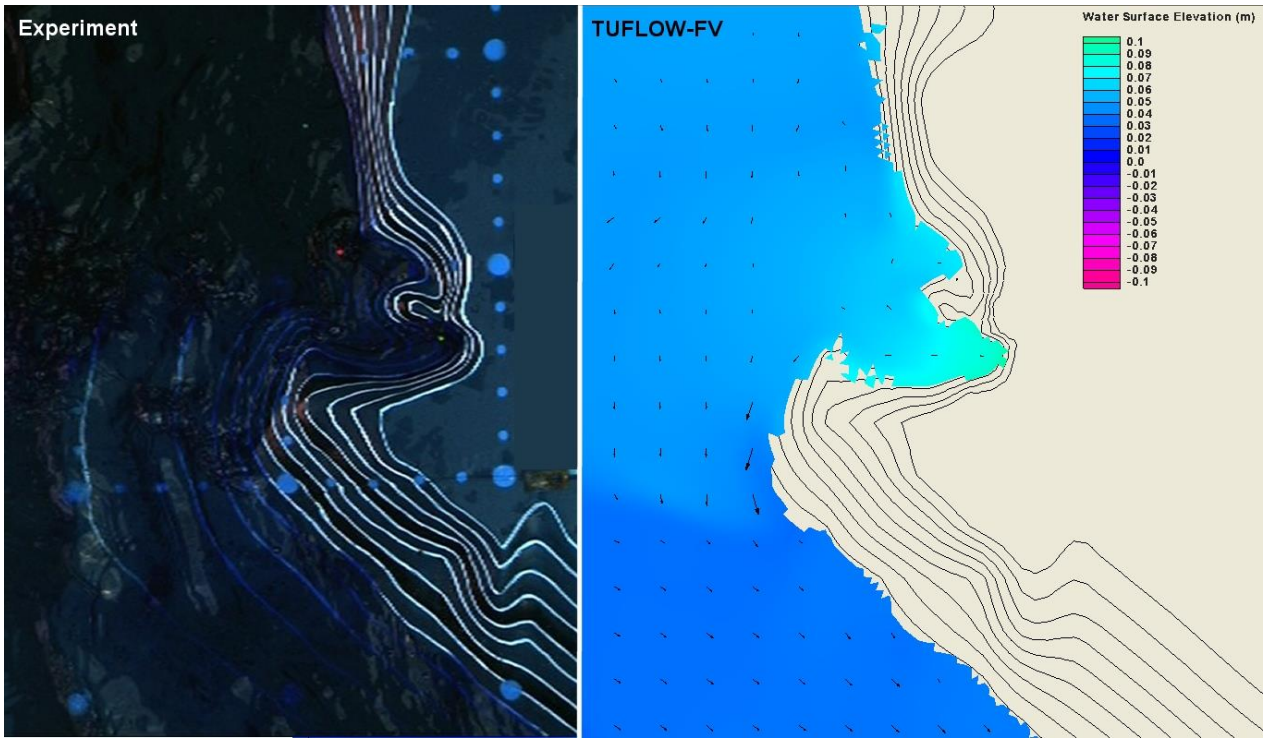

Figure 7 A snapshot of the modelled water surface at t = 17.1s compared to a video snapshot from the laboratory experiment

6 References

- Batten, P., C. Lambert and D.M. Causon, 1996. Positively Conservative High-Resolution Convection Schemes for Unstructured Elements. International Journal for Numerical Methods in Engineering; 39, 1821-1838.
- Brufau, P., Garcia-Navarro, P. and Vazquez-Cendon, M.E., 2004. Zero mass error using unsteady wetting–drying conditions in shallow flows over dry irregular topography. International Journal for Numerical Methods in Fluids; 45, 1047-1082.
- Chow, V.T., 1959. Open Channel Hydraulics. MacGraw-Hill Book Company Incorporation: New York.
- Falconer, R.A., B. Lin and S.M. Kashefipour, 2005. Modelling water quality processes in estuaries; published in Computational Fluid Dynamics: Applications in Environmental Hydraulics. John Wiley & Sons.
- Fisher, H.B., E.J. List, R.C.Y. Koh, J. Imberger and N.H. Brooks, 1979. Mixing in Inland and Coastal Waterways. Academic Press.
- Fringer, O.B., S.W. Armfield and R.L. Street, 2005. Reducing numerical diffusion in interfacial gravity wave simulations. International Journal for Numerical Methods in Fluids; 49, 301-329.
- Hubbard, M.E., 1999. Multidimensional Slope Limiters for MUSCL-Type Finite Volume Schemes on Unstructured Grids. Journal of Computational Physics, 155, 54–74.
- Hubbard, M.E. and P. Garcia-Navarro, 2000. Flux Difference Splitting and the Balancing of Source Terms and Flux Gradients. Journal of Computational Physics; 165, 89–125.
- Leveque, R.J., 2002. Finite Volume Methods for Hyperbolic Problems. Cambridge University Press.
- Munk, W. H., and E. R. Anderson, 1948. Notes on the theory of the thermocline,.*Journal of Marine Research, 3*, 276-295.
- Murillo, J., J. Burguete, P. Brufau¶ and P. Garcia-Navarro, 2005. Coupling between shallow water and solute flow equations: analysis and management of source terms in 2D. International Journal for Numerical Methods in Fluids; 49, 267-299.
- Murillo, J., P. Garcia-Navarro, J. Burguete and P. Brufau, 2006. A conservative 2D model of inundation flow with solute transport over dry bed. International Journal for Numerical Methods in Fluids; 52, 1059–1092.
- Roe, P.L., Approximate Riemann solvers, parameter vectors and difference schemes. Journal of Computational Physics, 43, 357-372.
- Rossmanith, J.A. D.S. Bale, R.J. LeVeque, 2004. A wave propagation algorithm for hyperbolic systems on curved manifolds. Journal of Computational Physics; 199, 631-662.
- Shchepetkin, A. F. and J. C. McWilliams, 2005. The regional oceanic modeling system (ROMS): a split-explicit, free-surface, topography-following-coordinate oceanic model. Ocean Modelling 9 (4), 347-404.
- Wu, J., 1980. Wind-stress coefficients over sea surface and near neutral conditions – A revisit. Journal of Physical Oceanography, 10, 727-740.

- Wu, J., 1982. Wind-stress coefficients over sea surface from breeze to hurricane. Journal of Geophysical Research; 87, C12, 9704-9706.